# Automatic Line Drawing Generation for Grotto Wall Surfaces Based on Depth Map and Normal Map Fusion

Jiteng Wang[1], Miaole Hou[1,2], Yong He[1,3], Bo Ning[3]

[1] School of Geomatics and Urban Spatial Informatics, Beijing University of Civil Engineering and Architecture, No. 15, Yongyuan Road, Huangcun Town, Daxing District, Beijing, 102627, China - 2108570424045@stu.bucea.edu.cn, houmiaole@bucea.edu.cn, 18734686621@163.com
[2] School of Land Engineering, Chang’an University, Middle Section, South 2nd Ring Road, Xi'an, Shaanxi, 710054, China - houmiaole@bucea.edu.cn
[3] Yungang Research Institute, No. 1, Dong Street, Yungang Town, Yungang District, Datong City, 037007, China - 18734686621@163.com; 40970156@qq.com

**Keywords:** Grotto wall surfaces; Line drawing; Depth map; Normal map; Mesh model

## Abstract

To address the lack of suitable methods for automatic 2D line drawing generation from grotto wall mesh models, as well as the difficulty of existing methods in balancing structural representation and detail preservation, this paper proposes a line drawing generation method based on depth map and normal map fusion. The method first orthographically projects the 3D model into a depth map and a surface normal map, then constructs an initial line drawing pipeline based on projected edge fusion. A layered optimization strategy is further introduced to improve detail representation and result stability. Experiments on the mesh model of the north wall of Cave 18 at the Yungang Grottoes show that the projected edge fusion method is more suitable for overall structural representation, while the layered optimization method performs better in preserving weak structures and fine details. The proposed method effectively improves the quality of automatic 2D line drawing generation for grotto wall surfaces.

## 1. Introduction

Grotto temples are a typical type of Buddhist heritage architecture and have long been affected by multiple factors, including natural environmental erosion and human-induced damage, making it urgent to employ digital technologies for systematic preservation and scientific research (Wang et al., 2021; Gong et al., 2025). Archaeological line drawing is an important form of cultural heritage documentation and representation. Owing to its highly condensed mode of expression, it plays a significant role in archaeological recording, image interpretation, and digital organization (Zhang et al., 2018; Zeng et al., 2024). However, traditional line drawings rely on manual tracing, which is inefficient and highly subjective, making it difficult to meet the demands of large-scale digital documentation. Therefore, the automatic generation of 2D line drawings has become an important research direction in the digital representation of cultural heritage.

Existing methods for 2D line drawing generation can be broadly divided into two categories: those based on 2D images and those based on 3D models. Image-based methods rely on extracting lines from image edges, grayscale information, and texture features (Kumar et al., 2019). For objects such as grotto wall surfaces, which are characterized by rough surfaces, rich carved details, and evident local damage, methods relying solely on 2D image information are easily affected by shadows and noise, making it difficult to preserve key structural information in a stable manner. In contrast, existing 3D-model-based methods usually represent structure through surface normals and curvature (Tsuchie and Higashi, 2013), but in complex grotto scenarios they still tend to produce redundant lines, miss fine details, cause line displacement, and yield incomplete results. Therefore, existing methods still fall short of directly meeting the needs of automatic 2D line drawing generation for complex grotto objects.

To address the above issues, this paper takes the traditional feature line extraction method based on mesh normal variation as a comparison baseline and proposes a 2D line drawing generation method based on depth map and normal map fusion. On this basis, a multi-scale enhancement and confidence-gating mechanism is further introduced to hierarchically optimize the main structural layer and the detail layer, thereby improving the representation of key structures on grotto wall surfaces as well as the continuity and visual readability of the results.

## 2. Related Work

Line drawing generation based on 2D images mainly serves image abstraction and non-photorealistic rendering. Related studies have evolved from early edge detection and image segmentation toward improvements in structural organization and line quality. For example, Son et al. (2007) proposed simulating hand-drawn sketches through local line fitting. Kang et al. (2007) further introduced local direction-guided filtering to improve line continuity and suppress noise. On this basis, Wang et al. (2012) enhanced line stability by improving edge detection methods. For archaeological applications, Zhang et al. (2018) generated archaeological line drawings by combining edge tracing and medial-axis detection. Zeng et al. (2024) proposed a generative adversarial network based on multi-branch feature fusion (U²FGAN) to improve line drawing quality. Overall, although 2D methods are relatively mature for image abstraction, they still face difficulties in balancing structural accuracy, detail selection, and output stability for complex heritage objects.

Line drawing generation based on 3D models mainly extracts lines by exploiting the geometric structure and surface information of the object. DeCarlo et al. (2003) introduced suggestive contours, which enhance shape depiction through variations in surface curvature and established a geometry-feature-based technical route. In archaeological contexts, existing studies can be broadly divided into two categories. The first directly extracts geometric feature lines from 3D data. For example, Luo et al. (2011) proposed a multi-scale 3D line drawing method for grotto heritage. Gilboa et al. (2013) developed an automatic drawing system for complex archaeological artifacts based on salient directions and relief edge detection. Li et al. (2025) focused on noisy point clouds and achieved automatic archaeological line drawing generation for stone sculpture point clouds through feature point detection and curve growing. The second category focuses on generating auxiliary tracing results. For example, Pan et al. (2016) enhanced orthographic views using the normal and texture information of 3D models to assist archaeologists in manual tracing. Overall, the former category is sensitive to noise, local scale, and computational complexity, while the latter still relies on manual involvement. Neither can directly meet the demand for automatic 2D line drawing generation for complex grotto wall surfaces.

## 3. Methodology

Taking the mesh model of a grotto wall surface as input, this study first constructs a 2D projection-based representation, including a depth map and a normal map. It then generates an initial line drawing by fusing the depth edge response and the normal edge response. On this basis, an edge-preserving smoothing, multi-scale enhancement, main-structure/detail-layer decomposition, and confidence-gating mechanism is further introduced to hierarchically optimize the line drawing. The overall technical workflow of this study is shown in Figure 1.

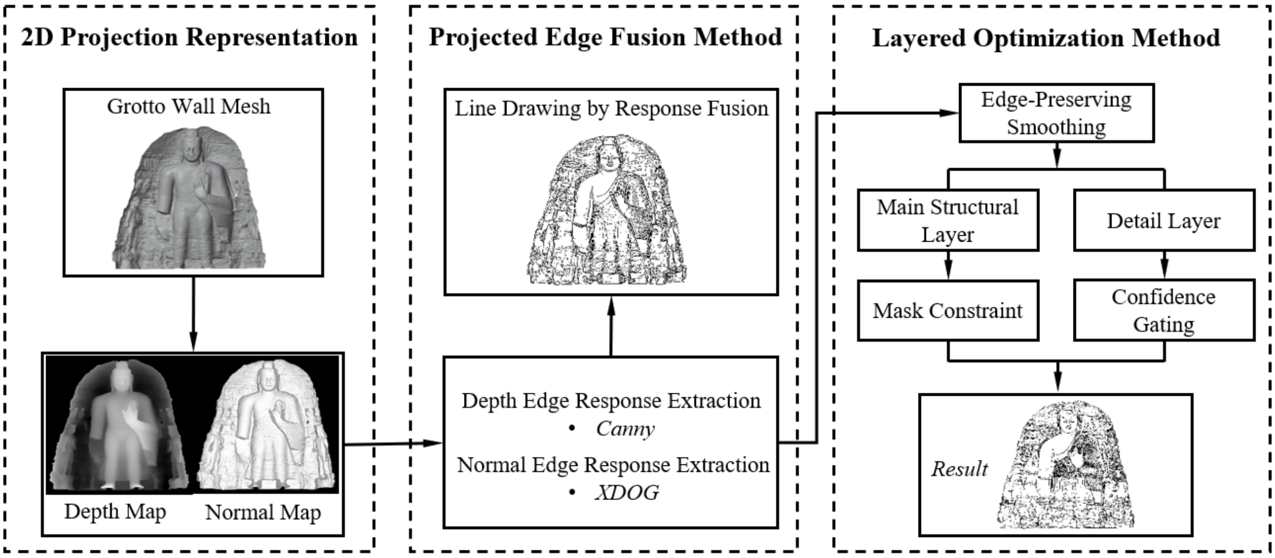


Figure 1. Overall technical workflow.

### 3.1 Construction of the 2D Projection-Based Representation

To convert the 3D model into a 2D representation suitable for subsequent line drawing extraction, the mesh vertices are first orthographically projected and then linearly mapped onto a 2D pixel grid, where depth maps and normal maps are generated through local point-splat rasterization. In this way, the geometric information of the 3D surface is uniformly transformed into the 2D representation required for subsequent line drawing generation.

The representation of vertex $p_i$ in the projection coordinate system is given in Eq. (1), where $c$ denotes the geometric center of the model; $u$ and $v$ denote the two orthogonal directions on the projection plane; and $w$ denotes the depth direction. $u_i$ and $v_i$ are the coordinates of the vertex on the projection plane, and $d_i$ is its projected value along the depth direction.

$$\tilde{p}_i = \begin{bmatrix} u_i \\ v_i \\ d_i \end{bmatrix} = \begin{bmatrix} u^\top (p_i - c) \\ v^\top (p_i - c) \\ w^\top (p_i - c) \end{bmatrix} \tag{1}$$

On this basis, by mapping the projection coordinates onto the pixel grid, a depth map reflecting the relief variations of the visible wall surface and a normal map describing surface orientation changes and local structural transitions can be generated. To reduce artifacts caused by projection holes, boundary discontinuities, and local sparsity, a valid-region mask is further constructed to constrain invalid areas and unstable boundary regions. Ultimately, the depth map, the normal map, and the valid-region mask together form the 2D representation foundation for subsequent line drawing generation.

### 3.2 Line Drawing Generation Based on Projected Edge Fusion

**3.2.1 Extraction of Depth Edge Response and Normal Edge Response**: During line drawing generation, the depth edge response and the normal edge response are first extracted from the 2D projection-based representation. The depth edge response is obtained by applying the Canny operator (Xu et al., 2024) to the depth map after Gaussian smoothing, and mainly reflects relief variations on the surface. The normal edge response is extracted from the normal map after smoothing using the eXtended Difference-of-Gaussians operator (Winnemöller et al., 2012), and mainly reflects local orientation changes. Together, they serve as the input for the subsequent edge response fusion.

The depth edge response $R_d$ is defined in Eq. (2), where $D$ denotes the depth map, $G_{\sigma d}(\cdot)$ denotes a Gaussian smoothing operator with scale parameter $\sigma d$, and $Canny(\cdot)$ denotes the Canny edge detector. This response mainly reflects the locations of depth discontinuities on the visible wall surface, and is therefore more effective for highlighting contour boundaries and large-scale structural transitions.

$$R_d = Canny\left(G_{\sigma d}(D)\right) \tag{2}$$

The normal edge response $R_n$ is obtained from the normal grayscale image $I_n$ through the eXtended Difference-of-Gaussians operator and a nonlinear mapping, as shown in Eq. (3), where $XDoG(\cdot)$ denotes the eXtended Difference-of-Gaussians operator. Compared with the depth edge response, the normal edge response is more suitable for capturing shallow surface details and weak structural cues.

$$R_n = XDoG\left(I_n\right) \tag{3}$$

To prevent invalid projection regions from interfering with feature extraction, the valid-region mask is further used to remove response values in invalid areas after the depth edge response map and the normal edge response map are generated.

**3.2.2 Edge Response Fusion and Line Drawing Generation**: After obtaining the depth edge response and the normal edge response, the two are fused into a unified response map by weighted combination, as shown in Eq. (4), where $\alpha$ and $\beta$ denote the weights of the depth edge response and the normal edge response, respectively. To emphasize the main contours of the wall surface and the boundaries of large-scale relief variations, a higher weight is assigned to the depth edge response than to the normal edge response.

$$R = \alpha R_d + \beta R_n \tag{4}$$

Considering that false contours are likely to occur near projection boundaries, a boundary attenuation mask is further introduced to suppress the response map by weighted modulation, so as to reduce unstable responses in boundary regions. Subsequently, local contrast enhancement and smoothing are applied to the response map to improve the distinguishability of weak lines and suppress scattered noise. Finally, the enhanced response map is binarized, as defined in Eq. (5), where $B(x,y)$ denotes the binarization result and $T$ denotes the segmentation threshold. The threshold $T$ is automatically determined using the Otsu method (Xiao et al., 2020). On this basis, an initial line drawing is generated by combining morphological closing, connected-component filtering, and skeletonization.

$$B(x,y) = \begin{cases} 1 & ,R'(x,y) \geq T \\ 0 & ,R'(x,y) < T \end{cases} \tag{5}$$

By integrating depth variation and normal variation information through a unified response fusion process, this method can generate a 2D line drawing in a relatively direct manner. However, since both the main structural cues and the detail cues still share the same response construction strategy and post-processing pipeline, there remains room for further improvement in hierarchical line representation.

### 3.3 Line Drawing Generation Based on Layered Optimization

**3.3.1 Edge-Preserving Smoothing and Multi-Scale Enhancement**: To suppress projection noise while preserving structural transitions and shallow details as much as possible, edge-preserving smoothing is first applied to the depth map and the normal map. Unlike the previous method, which uses Gaussian smoothing, the present method applies bilateral filtering (Durand and Dorsey, 2002) to the depth map and separately performs bilateral filtering on the three normal components, $N_u$, $N_v$, and $N_w$, so as to obtain a more stable input representation. Compared with Gaussian smoothing, bilateral filtering can better preserve main boundaries and local structural transitions while reducing local noise.

On this basis, the Sobel operator (Dastjerdi and Ahmad, 2025) is used to compute the depth gradient and the normal gradient, thereby constructing the enhanced depth edge response $E_d$ and the enhanced normal edge response $E_n$, respectively. To further enhance high-frequency structures such as shallow relief details and weak incisions, a multi-scale enhancement mechanism is introduced. Specifically, small-scale and large-scale smoothing are applied to the depth map and the normal map, and their difference is used to extract high-frequency information, thereby strengthening the expression of local details.

**3.3.2 Construction of the Main Structural Layer and the Detail Layer**: To overcome the limitation of a unified response map in simultaneously representing main contours and fine textures, the line drawing generation process is further divided into two branches: a main structural layer and a detail layer, which model large-scale structural information and local detail information, respectively. The main structural layer mainly emphasizes wall contours and component boundaries, while the detail layer focuses on the expression of shallow relief textures, local incisions, and weak boundaries.

The main structural layer $S_m$ is constructed by weighted combination of the depth edge response and the normal edge response, as shown in Eq. (6), where $\alpha_m$ and $\beta_m$ are the corresponding weights and satisfy $\alpha_m > \beta_m$, indicating that the main structural layer relies more on depth edge information.

$$S_m = \alpha_m E_d + \beta_m E_n \tag{6}$$

The detail layer further introduces multi-scale high-frequency enhancement on the basis of basic edge fusion, as shown in Eq. (7), where $S_d$ denotes the basic detail response; $\alpha_d$ and $\beta_d$ are the weights of the depth edge response and the normal edge response, respectively, with $\beta_d > \alpha_d$; $H_d$ denotes the depth high-frequency term, and $H_n$ denotes the normal high-frequency term; $\lambda_1$, $\lambda_2$, and $\lambda_3$ control the contributions of the basic detail response, the normal high-frequency term, and the depth high-frequency term, respectively.

$$S_d = \lambda_1(\alpha_d E_d + \beta_d E_n) + \lambda_2 H_n + \lambda_3 H_d \tag{7}$$

In addition, considering that false responses caused by projection sparsity are likely to occur near boundaries, both the main structural layer and the detail layer are constrained by an internal mask in boundary regions, so as to suppress unstable responses and reduce interference from false lines.

**3.3.3 Confidence-Constrained Line Optimization**: Since the detail layer is more sensitive to surface noise and local disturbances, a confidence-gating mechanism is further introduced to filter detail cues. Specifically, a detail cue is retained only when a pixel simultaneously satisfies certain conditions on the normal edge response and the depth edge response, or when its normal high-frequency response is sufficiently significant. The gating function is defined in Eq. (8), where $M_c(x,y)$ denotes the confidence-gating result at pixel $(x,y)$, and $T_n$, $T_d$, and $T_h$ denote the corresponding decision thresholds.

$$M_c(x,y)=\begin{cases}1, & (E_n > T_n \wedge E_d > T_d) \vee (H_n > T_h) \\ 0, & otherwise\end{cases} \tag{8}$$

On this basis, percentile thresholds are applied to binarize the main structural layer and the detail layer, respectively, so as to adapt to the distribution differences of responses at different levels. In the subsequent line post-processing stage, the main structural layer emphasizes completeness and continuity; therefore, false lines are further removed and curve smoothing is performed after morphological closing and connected-component filtering. In contrast, the detail layer is skeletonized after a light morphological closing operation, and a relatively looser connected-component filtering strategy is adopted to preserve local incisions and weak textures as much as possible. Meanwhile, the outermost contour is extracted separately from the valid projection region, and then independently smoothed and moderately thickened to enhance the clarity of the overall boundary.

Finally, the outer contour, the main structural layer, and the detail layer are fused to obtain the final line drawing result $L$, as shown in Eq. (9), where $L_o$, $L_m$, and $L_d$ denote the results of the outer contour, the main structural layer, and the detail layer, respectively.

$$L = L_o \cup L_m \cup L_d \tag{9}$$

## 4. Results and Discussion

### 4.1 Experimental Data

The experimental dataset used in this study is a 3D mesh model of the north wall of Cave 18 at the Yungang Grottoes. This area contains rich carved elements, diverse Buddha figures, and a complex surface structure, featuring main contours, shallow relief details, and local texture variations. It is therefore highly representative and suitable for testing and validating line drawing generation methods for complex grotto wall surfaces.

The mesh model used in the experiments was generated from point cloud data through preprocessing steps including registration, denoising, and resampling, followed by surface reconstruction (Yang et al., 2022). Since the original reconstructed model still contained noticeable noise in some local areas, additional smoothing optimization was applied to regions with concentrated noise. The final mesh model of the north wall of Cave 18 is shown in Figure 2.

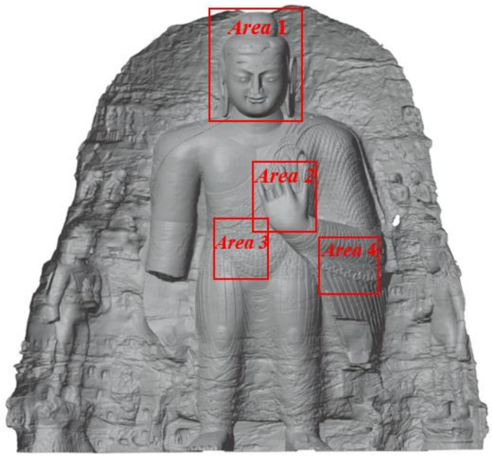


Figure 2. Mesh model of the north wall of Cave 18 at the Yungang Grottoes with selected local regions

### 4.2 Comparison of Line Drawing Generation Results

To validate the effectiveness of the proposed method, a traditional feature line extraction method based on normal variation was selected as the comparison baseline, and was compared with the projected edge fusion method and the further layered optimization method.

Figure 3 shows the overall line drawing results of the north wall mesh model of Cave 18 under the three methods. From the overall results, although the traditional normal-variation-based method can extract certain structural cues, the resulting line segments are relatively scattered, with many redundant lines, and the overall continuity and regularity are insufficient. In contrast, the projected edge fusion method better combines depth variation and normal variation information, producing line drawings with stronger continuity, clearer main contours and major structural boundaries, and a cleaner and more stable overall result. With further layered optimization, local details are further enhanced while maintaining the readability of the overall structure.

To compare the performance of different methods in local regions more clearly, four representative local regions were selected from the mesh model, as shown in Figure 2. These regions correspond to different types of structural features, including the main facial area, the hands in front of the chest, torso folds, and the Thousand-Buddha kasaya pattern. Figure 4 presents enlarged comparisons of these typical local regions. It can be seen that the traditional normal-variation-based method produces relatively disordered line organization and fails to form a regular line drawing representation. The projected edge fusion method achieves better continuity and cleanliness, but its extraction of weak detail structures such as the Thousand-Buddha kasaya pattern remains insufficient. In contrast, the layered optimization method preserves the Thousand-Buddha kasaya pattern and other fine details more completely, indicating stronger capability in representing weak structures and high-frequency details. However, it also introduces more fragmented lines, making the overall result slightly less clean than that of the projected edge fusion method.

Overall, the projected edge fusion method is more suitable for generating clear and regular overall line drawings, whereas the layered optimization method performs better in local detail and weak-feature representation.

(a) Traditional normal-variation-based method (b) Projected edge fusion method (c) Layered optimization method

Figure 3. Comparison of the overall line drawing results of the three methods

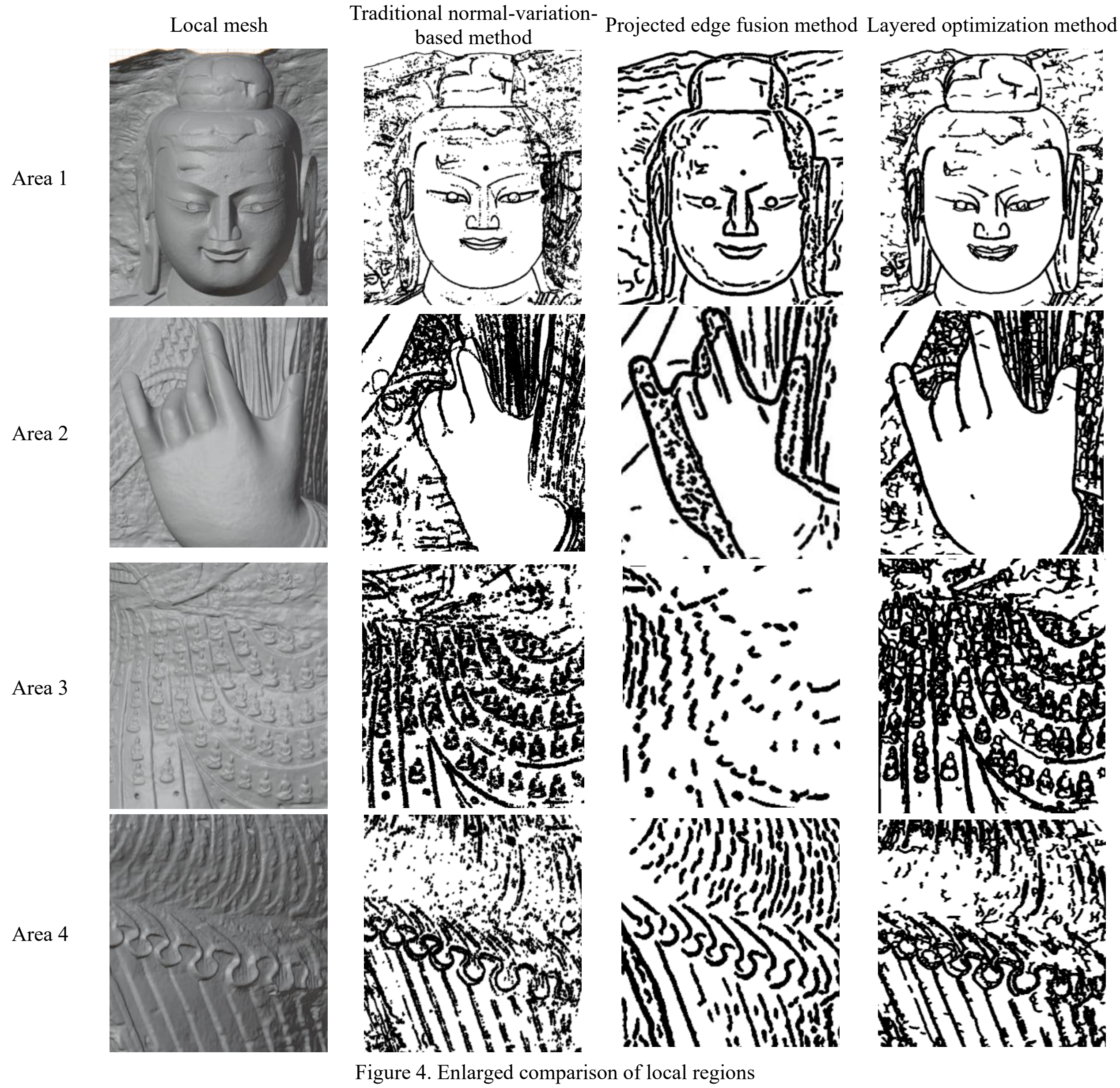


Figure 4. Enlarged comparison of local regions

### 4.3 Evaluation Metrics and Quantitative Results

To evaluate the effectiveness of the generated line drawings, this study adopts a full-image valid-region evaluation strategy under a unified projection space, and performs a no-reference quantitative comparison of the line drawings produced by different methods. Considering the complex structure and rich detail hierarchy of grotto wall surfaces, constructing complete reference line drawings manually is both costly and highly subjective. Therefore, instead of using accuracy evaluation based on ground-truth annotations, this study defines four no-reference evaluation metrics by combining curvature distribution and line topology characteristics: High-curvature Support Ratio (HSR), High-curvature Coverage Ratio (HCR), Flat-region Line Ratio (FLR), and Line Fragmentation Index (FI).

Specifically, HSR measures the degree to which the extracted lines conform to high-curvature structures, as defined in Eq. (10). HCR measures the extent to which high-curvature structures are covered by the extracted lines, as defined in Eq. (11). FLR measures the proportion of redundant lines in low-curvature flat regions, as defined in Eq. (12). FI measures the fragmentation degree of the extracted lines, as defined in Eq. (13). HSR, HCR, and FLR are all ratio-based metrics ranging from 0 to 1, while FI is defined as the ratio between the number of skeletal connected components and the total skeleton length, and also falls within the range of [0,1] in the present experiments. In general, higher HSR and HCR values indicate more sufficient response to and coverage of valid structures, whereas lower FLR and FI values indicate fewer false lines in flat regions and better line continuity. In these equations, $L$ denotes the set of line pixels, $H_{\tau h}$ denotes the high-curvature region, $D_r(\cdot)$ denotes the tolerance neighborhood, $S$ denotes the skeleton set of the extracted lines, $|s|$ denotes the total skeleton length, and $N_c$ denotes the number of skeletal connected components.

$$HSR = \frac{|L \cap D_r(H_{\tau h})|}{|L|} \tag{10}$$

$$HCR = \frac{|H_{\tau h} \cap D_r(L)|}{|H_{\tau h}|} \tag{11}$$

$$FLR = \frac{|L \cap F_{\tau l}|}{|L|} \tag{12}$$

$$FI = \frac{N_c}{|S|} \tag{13}$$

Table 1 presents the quantitative evaluation results of the traditional normal-variation-based method, the projected edge fusion method, and the further layered optimization method. The traditional method achieves HSR and HCR values of 0.868 and 0.986, respectively, indicating strong responsiveness to high-curvature structures and high coverage of such regions. However, its FLR and FI reach 0.148 and 0.036, respectively, suggesting a relatively large number of false lines in flat regions and a higher degree of line fragmentation. In contrast, the projected edge fusion method reduces FLR and FI to 0.048 and 0.022, respectively, demonstrating better performance in terms of line purity and continuity. Nevertheless, its HSR and HCR are 0.710 and 0.628, indicating relatively insufficient conformity to and coverage of high-curvature structures. The layered optimization method shows better overall performance across all four metrics: its HSR reaches 0.917, the highest among the three methods, while its HCR remains at a relatively high level of 0.855. Its FLR and FI are 0.058 and 0.008, respectively, with FI being the lowest, indicating that this method further improves line continuity and reduces fragmentation while maintaining strong structural responsiveness. Overall, the traditional method emphasizes structural coverage, the projected edge fusion method favors false-line suppression and overall cleanliness, whereas the layered optimization method achieves a better balance among structural conformity, false-line control, and line organization.

| Method | HSR | HCR | FLR | FI |
|---|---|---|---|---|
| Traditional normal-variation-based method | 0.868 | 0.986 | 0.148 | 0.036 |
| Projected edge fusion method | 0.710 | 0.628 | 0.048 | 0.022 |
| Layered optimization method | 0.917 | 0.855 | 0.058 | 0.008 |

Table 1. Evaluation Results

## 5. Conclusion and Future Work

This study addresses the problem of automatic 2D line drawing generation for grotto wall mesh models by proposing a line drawing generation method based on depth map and normal map fusion. The method first orthographically projects the 3D model into a depth map and a normal map, on the basis of which an initial line drawing generation pipeline based on projected edge fusion is constructed. It further introduces edge-preserving smoothing, multi-scale enhancement, main structure and detail layer decomposition, and a confidence-gating mechanism to achieve layered optimization of line drawing generation. Compared with the traditional feature line extraction method based on normal variation, the proposed method better integrates depth variation and surface orientation variation, thereby improving line continuity and result stability while maintaining the readability of the overall structure.

Experimental results show that the projected edge fusion method can generate overall line drawings that are relatively clear, regular, and clean, making it suitable for scenarios requiring strong representation of main contours and overall structures. The further layered optimization method performs better in expressing weak structures, shallow relief textures, and local incisions, and can preserve fine details such as the Thousand-Buddha kasaya pattern more completely. Quantitative evaluation further demonstrates that the layered optimization method achieves a better balance among high-curvature structure conformity, false-line suppression, and line continuity, thereby verifying the effectiveness of the proposed method for automatic line drawing generation on complex grotto wall surfaces.

At the same time, some limitations remain. For example, while layered optimization enhances local details, it may also introduce more fragmented fine lines. In addition, some parameters still need to be adjusted according to object characteristics, indicating that the adaptability of the method can be further improved. Future work will focus on adaptive parameter selection strategies for different types of grotto wall surfaces, as well as more robust structural constraints and post-processing mechanisms, so as to achieve a better balance between detail representation and overall cleanliness. Further validation on more diverse samples will also be conducted to evaluate the robustness and general applicability of the method.

## Acknowledgements

We acknowledge grants from the National Natural Science Foundation of China (No.42171444).

## References

DeCarlo, D., Finkelstein, A., Rusinkiewicz, S., Santella, A., 2003. Suggestive contours for conveying shape. ACM Transactions on Graphics, 22(3), 848–855. doi.org/10.1145/882262.882354.

Durand, F., Dorsey, J., 2002. Fast bilateral filtering for the display of high-dynamic-range images. ACM Transactions on Graphics, 21(3), 257–266. doi.org/10.1145/566654.566574.

Gilboa, A., Tal, A., Shimshoni, I., Kolomenkin, M., 2013. Computer-based, automatic recording and illustration of complex archaeological artifacts. Journal of Archaeological Science, 40, 1329–1339. doi.org/10.1016/j.jas.2012.09.018.

Gong, Y., Wang, X., Wang, S., Lin, W., Jin, K., 2025. Impact of open visits on the indoor climate of Mogao Caves. npj Heritage Science, 13, 173.

Kang, H., Lee, S., Chui, C.K., 2007. Coherent line drawing. In: Proceedings of the 5th International Symposium on Non-Photorealistic Animation and Rendering (NPAR '07), 43–50. doi.org/10.1145/1274871.1274878.

Kumar, M.P.P., Poornima, B., Nagendraswamy, H.S., Manjunath, C., 2019. A comprehensive survey on non-photorealistic rendering and benchmark developments for image abstraction and stylization. Iranian Journal of Computer Science, 2, 131–165.

Li, J., Yang, J., Han, G., Wu, H., Zhu, J., Cui, H., 2025. Automated generation of archeological line drawings from sculpture point cloud based on weighted centroid projection. npj Heritage Science, 13, 162.

Luo, T., Li, R., Zha, H., 2011. 3D line drawing for archaeological illustration. International Journal of Computer Vision, 94, 23–35. doi.org/10.1007/s11263-010-0394-y.

Pan, R., Tang, Z., Xu, S., Da, W., 2017. Normals and texture fusion for enhancing orthogonal projections of 3D models. Journal of Cultural Heritage, 23, 33–39. doi.org/10.1016/j.culher.2016.07.009.

Salehi Dastjerdi, N., Ahmad, M.O., 2025. Depth Upsampling with Local and Nonlocal Models Using Adaptive Bandwidth. Electronics, 14(8), 1671. doi.org/10.3390/electronics14081671.

Son, M., Kang, H., Lee, Y., Lee, S., 2007. Abstract line drawings from 2D images. In: 15th Pacific Conference on Computer Graphics and Applications (PG'07), Maui, HI, USA, 333–342. doi.org/10.1109/PG.2007.63.

Tsuchie, S., Higashi, M., 2014. Extraction of surface-feature lines on meshes using normal tensor framework. Computer-Aided Design and Applications, 11(2), 172–181. doi.org/10.1080/16864360.2014.846088.

Wang, S., Wu, E., Liu, Y., Liu, X., Chen, Y., 2012. Abstract line drawings from photographs using flow-based filters. Computers & Graphics, 36, 224–231.

Wang, X., Wang, Y., Guo, Q., Pei, Q., Zhao, G., 2021. The history of rescuing reinforcement and the preliminary study of preventive protection system for the cliff of Mogao Grottoes in Dunhuang, China. Heritage Science, 9, 58.

Winnemöller, H., Kyprianidis, J.E., Olsen, S.C., 2012. XDoG: An eXtended difference-of-Gaussians compendium including advanced image stylization. Computers & Graphics, 36(6), 740–753.

Xiao, L., Ouyang, H., Fan, C., 2020. Otsu’s thresholding method based on plane intercept histogram and geometric analysis. The International Arab Journal of Information Technology, 17, 692–701. doi.org/10.34028/iajit/17/5/2.

Xu, J., Niu, S., Wang, Z., 2024. Object tracking method based on edge detection and morphology. EURASIP Journal on Advances in Signal Processing, 2024, 45.

Yang, S., Xu, S., Huang, W., 2022. 3D point cloud for cultural heritage: A scientometric survey. Remote Sensing, 14(21), 5542. doi.org/10.3390/rs14215542.

Zeng, X., Cheng, L., Li, S., Liu, X., 2024. An algorithm based on multi-branch feature cross fusion for archaeological illustration of murals. Heritage Science, 12, 368.

Zhang, J., Liu, Z., Liu, S., 2019. Computer simulation of archaeological drawings. Journal of Cultural Heritage, 37, 181–191. doi.org/10.1016/j.culher.2018.11.014.